Ceramics International 46 (2020) 17103–17111

Contents lists available at ScienceDirect

Ceramics International

journal homepage: www.elsevier.com/locate/ceramint

Enhanced performance of AA7150-SiC nanocomposites synthesized by novel fabrication process

Pagidi Madhukar[a,*], N. Selvaraj[a], C.S.P. Rao[b], G.B. Veeresh Kumar[c]

[a] Department of Mechanical Engineering, National Institute of Technology - Warangal, Warangal 506004, Telangana State, India
[b] National Institute of Technology - Andhra Pradesh, Tadepalligudem - 534101, West Godavari District, Andhra Pradesh State, India
[c] Department of Mechanical Engineering, National Institute of Technology - Andhra Pradesh, Tadepalligudem - 534101, West Godavari District, Andhra Pradesh State, India

ARTICLE INFO

Keywords:
SiC
AA7150
Double stir casting
Ultrasonic
Microstructure
Mechanical properties
Nanocomposites
Grain refinement

ABSTRACT

This research has successfully introduced a novel fabrication process to manufacture aluminium alloy (AA)7150-X wt.% silicon carbide (SiC) (X = 0.5, 1.0, 1.5, and 2.0) nanocomposites. The effect of silicon carbide nanoparticle content on microstructure, density, microhardness, porosity and ultimate tensile strength was studied. An optical microscope was used to find the grain formation while electron microscopy was used for ceramic nanoparticle distribution studies and fractographic studies of fracture surface. Energy Dispersive X-Ray Spectroscopy and X-ray diffraction were used to study the chemical composition of various composites and SiC particles. Significant enhancement was observed in mechanical properties at as-cast state of composites. Nevertheless, AA7150–1.5%SiC nanocomposite exhibited 83.47% reduction in porosity, 23.9% enhancement in microhardness, 60.1% in ultimate tensile strength compared to base alloy.

1. Introduction

Aerospace and automobile sectors are always in search of new materials with higher grade mechanical and wear properties along with ease of fabrication and the ability to vary composition so that a range of desired properties may be attained. Lightweight, high stiffness, and high strength make aluminium (Al)–Zinc (Zn)–Copper (Cu)–Magnesium (Mg) alloy metal matrix composite (MMCs) a suitable candidate material for aerospace, military and automobile applications. Ceramic micro-particulates are injected into aluminium metal alloy to enhance its mechanical and wear properties but in recent years, nanoparticles have been introduced to fabricate metal matrix nanocomposites and these exhibit far better properties than micro composites which has been confirmed by positive results, especially with respect to strength, corrosion resistance, wear resistance, fatigue life of the material and temperature creep resistance [1–5].

Silicon carbide is the most commonly used particulate reinforcement for aluminium alloy matrix because it is widely available at affordable price and displays high hardness. Particulates can be easily reinforced to fabricate metal matrix composites compared to continuous reinforcements and have low production cost compared to fiber reinforced composites. The dispersion of nanoscale particles in molten liquid is very difficult with conventional methods due to high surface area to volume and this plays a key role for uniform dispersion of nanoparticles in dense liquid metal to produce high quality nanocomposites. Vortex method has been introduced to avoid the floating of nanoparticle on liquid metal surfaces. The incorporation of ceramic nanocomposites leads to the agglomerations in liquid metal. These agglomerations act as a crack initiator and propagate crack growth which leads to premature failure of nanocomposites.

Several methods are available to manufacture aluminium based nanocomposites. Among them, liquid state stir casting process was seen to be the most powerful technique for dispersion of nanoparticles that could be produced with large capacity and low cost [6]. Ultrasonic vibration is one of the best techniques for degassing, and purifying liquid Al melt [7,8], refinement of nanocomposites at microstructure level [9,10], and ensuring uniform distribution of nanoparticles [11]. Yang et al [11] found that ultrasonic vibration treatment was also a highly effective technique to distribute ceramic nanoparticles in molten liquid because of acoustic streaming and cavitation effect. The ultrasonic energy introduces cavitation bubbles which develop micro level “hot spots” containing high temperature and pressure. Hence, these can break up the agglomerations and enhance the wettability of nanoparticles in the molten liquid of Al alloy. In the meantime, acoustic streaming stimulates homogeneous mixing of ceramic nanoparticles in the metal pool. Amin Bahrami et al [12] studied the wettability,

* Corresponding author.
E-mail address: pmadhu88@gmail.com (P. Madhukar).

https://doi.org/10.1016/j.ceramint.2020.04.007
Received 16 December 2019; Received in revised form 26 March 2020; Accepted 1 April 2020
Available online 08 April 2020

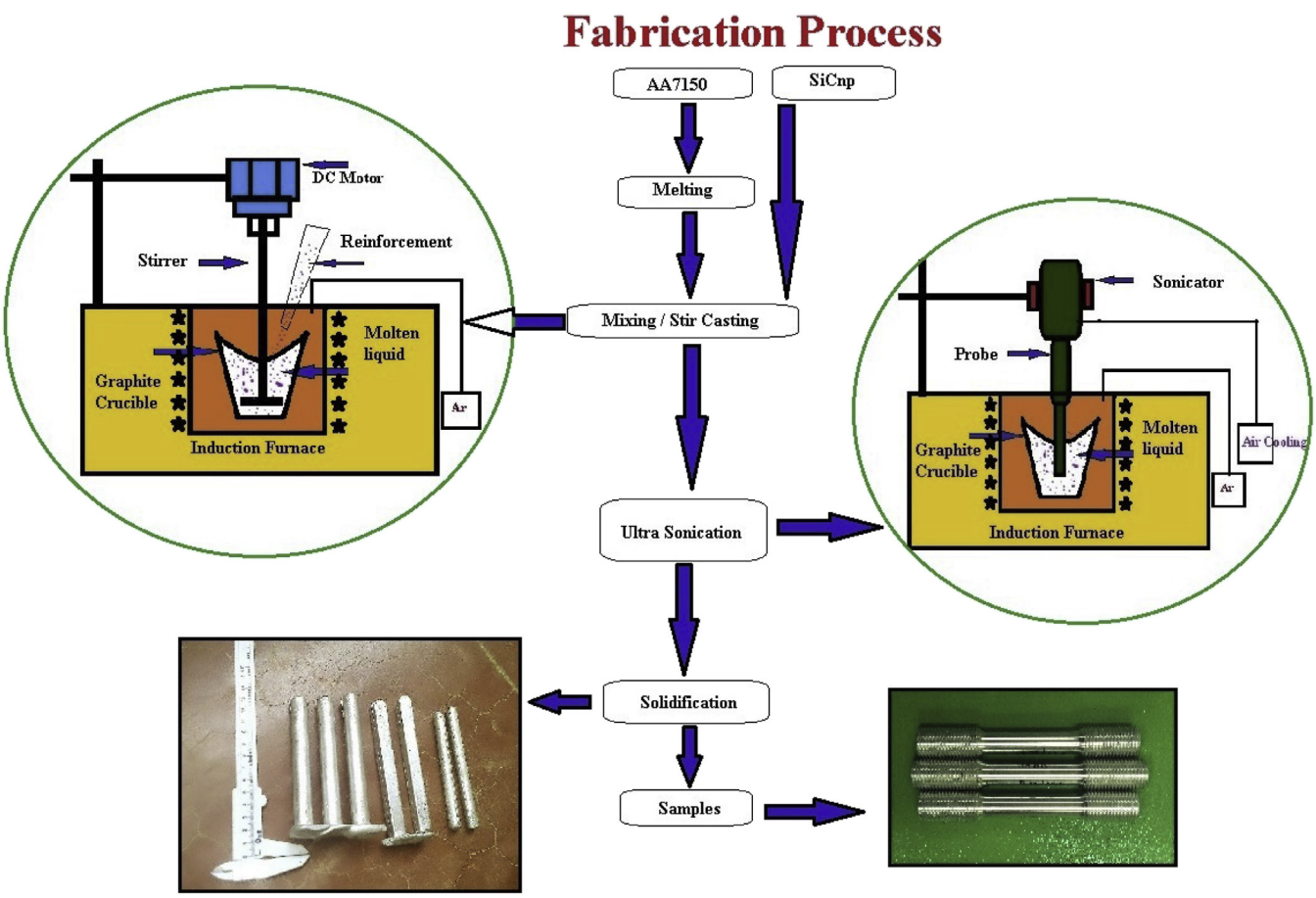

Fig. 1. Fabrication process with materials, stirring, sonication and spaceman's.

thermal and electrical behavior of Boron carbid (B_4C)/crystalline rice husk ash (RHA) as well as B_4C/amorphous RHA reinforced aluminium matrix composites (AMCs). From the results it is observed that the addition of RHA (amorphous or crystalline) shown good wettability with Al-alloy liquid metal.

Du Yuan et al [13] studied the effect of squeeze casting and ultrasonic vibration techniques for reinforcement and the effect of SiC nanoparticle distribution of A356-2 wt%SiC nanocomposites. It is observed that ultrasonic treatment (3 min) reduces secondary dendritic arm spacing of α-Al by 49% while it also reduces squeeze casting by 55% compared to base A356 alloy matrix. Knowles et al [14] and Kolo [15], applied liquid stir casting technique to the mixing of ceramic reinforcements. A mechanical stirrer was used to disperse nanoparticles and the difficulty faced during the mixing of nanoparticles was evident due to the large specific surface area of ceramic nanoparticles. Therefore, supporting process is required to enhance uniform distribution of ceramic nano reinforcement particles in the melt pool. Jianyu et al [16] investigated the influence of ultrasonic vibration effect on 10 wt% Magnesium silicide (Mg_2Si)-1 wt% SiC_{np}-Al-Cu hybrid composite and analyzed the mechanical properties. It was observed that ultrasonic treatment enhanced the ultimate strength of a hybrid composite by 33.5% compared to base alloy matrix. Idrisi et al [17] developed AMCs using conventional and ultrasonic vibration assisted stir casting as well as demonstrated the drawbacks of conventional method over a ultrasonic vibration assisted stir casting. These drawbacks were eliminated by ultrasonic energy during the sonication process in the molten metal. Moreover, the microstructural studies disclosed the homogeneous dispersion of SiC micro-particles and enhanced mechanical properties while using ultrasonic vibration assisted stir casting technique. Madhukar et al [18] successfully investigated the ultrasonic vibration treatment effect on AA7150-SiC nanocomposite and compared with double stir casting method. It was found that the mechanical strength and microstructure properties were enhanced as well as achieved uniform dispersion of nanoparticles while comparing with double stir casting method.

In this research, a novel fabrication process was successfully developed and introduced by combining a sequence of vortex, two step stir casting and ultrasonication techniques to ensure homogeneous distribution of nanoparticles, leading to refinement of microstructure in the nanocomposites. The mechanical properties, microstructure analysis for grain refinement, particle distribution and fractography of AA7150-SiC nanocomposites were also investigated.

2. Materials and methods

AA7150 ingot was chosen as matrix material and bought from Venuka Engg. Pvt. Ltd., Hyderabad, India. SiC nanoparticles were chosen for reinforcements, with a density of 3.216 g/cc, > 99.9% purity and average particle size (APS) of 40–60 nm. It was procured from Platonic Nanotech Pvt. Ltd., Jharhand, India.

The experimental setup for the fabrication process is shown in Fig. 1. AA7150 ingot was melted and maintained at 750 °C for an hour to achieve uniform melting throughout the liquid. A mechanical stirrer was placed into the melt and stirring action was performed for 20 min in two steps. While stirring, 1% coarse Mg powder was added to improve the wettability of SiC nanoparticles and Hexachloroethane - C_2Cl_6 for degassing. Preheated (500 °C) nano SiC particles (0.5, 1.0, 1.5, 2.0 wt% SiC) were added in the melt pool and two double stir casting process was performed followed by ultrasonic assisted vibration for 10 min. The fabricated molten liquid was poured into preheated

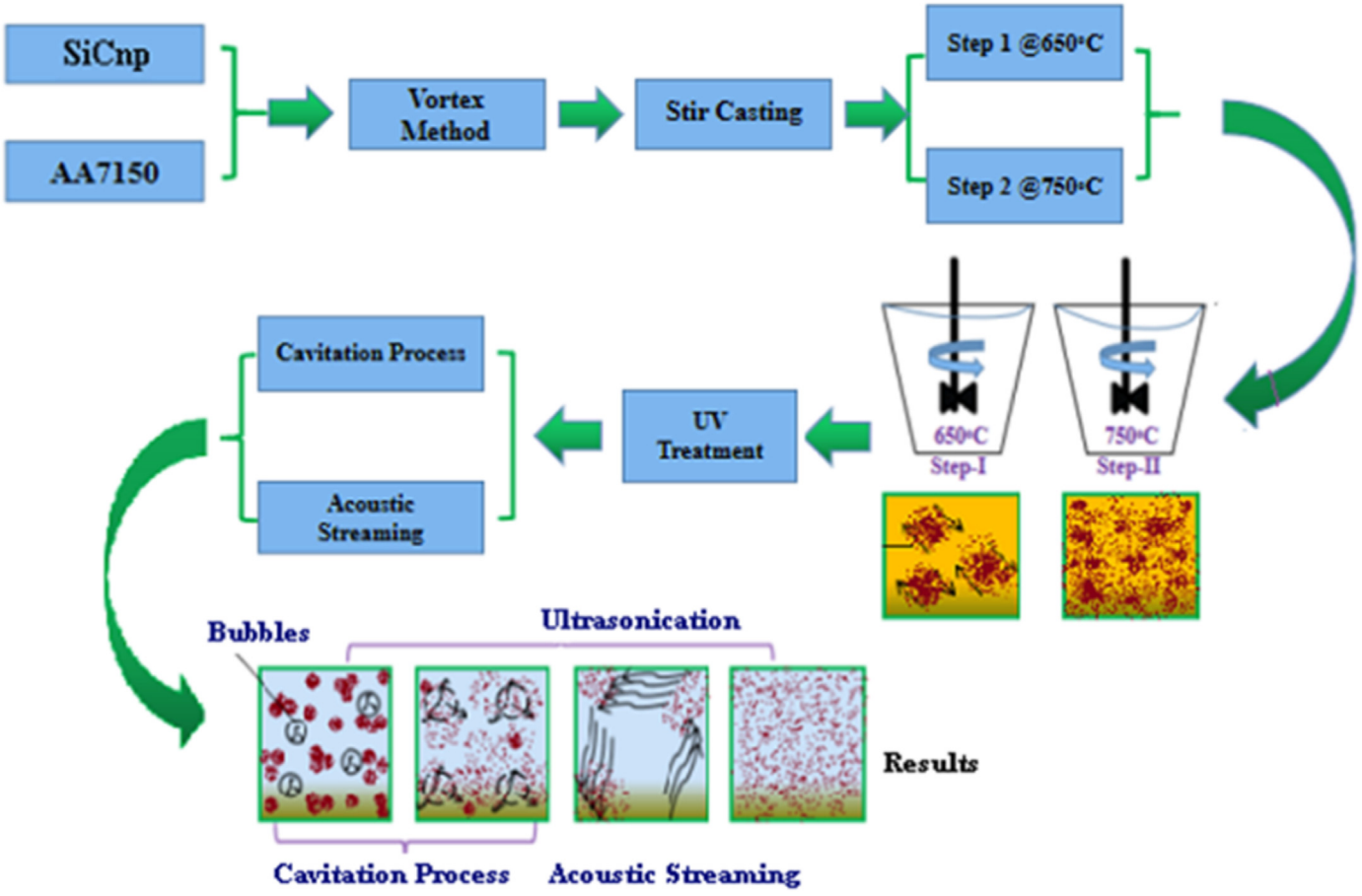

Fig. 2. Schematic diagram for detailed mechanism of novel fabrication process.

Table 1
Average Grain Size (AGS) and mechanical properties of nanocomposites and base alloy matrix.

Composition	Ex-Density (g/cc)	AGS (μm)	Porosity (%)	UTM (MPa)	Hardness (HV)
AA7150	2.725573	152	3.69	114	151.8
AA7150–0.5%SiC	2.763739	101	2.4	131	168.2
AA7150–1.0%SiC	2.787498	73	1.62	143.7	172.76
AA7150–1.5%SiC	2.817805	64	0.61	182.5	188.1
AA7150–2.0%SiC	2.825773	113	0.775	169	177.72

(500 °C) mold and allowed to cool for 24 h at room temperature.

2.1. Detailed mechanism for novel fabrication process

A novel fabrication process was developed to produce homogeneous mixing of SiC nanoparticles throughout the Al melt pool and the schematic line diagram is represented in Fig. 2. This fabrication process involves a combination of three techniques, namely vortex method, double stir casting method and ultrasonic vibration method. Vertex method was conducted at 750 °C temperature (above liquidus) to increase the flowability of liquid as well as particles redirected into liquid metal. Double stir casting method was a two step stirring process that used mechanical rotary impeller. Each step involved 10 min of stirring process. Step-I: It was performed at 650 °C for 10 min leading to a reduction in the agglomerations due to the high viscosity of material at a lower temperature. This led to break up of the agglomeration because of high frictional forces between the reinforcements and matrix. Then molten liquid was allowed to become semi-solid. Step-II: It was performed at 750 °C above liquidus temperature and it allowed distribution of ceramic nanoparticles due to the liquid property of high flowability and low viscosity at higher temperatures. Finally, ultrasonic vibration was also performed above liquidus temperature because of the high flowability of the nanoparticles with low viscosity, where ultrasonic energy waves transferred effectively through liquid pool leading to the creation of cavities and acoustic streaming. The cavitation bubbles are produced at high temperature (> 5000 °C) along with high pressure (> 1000 atm). Due to the transient difference in pressure and temperature, the bubbles collapse and break the nano agglomerations. Meanwhile, the acoustic stream spreads the nanoparticles into liquid metal and the combined effect of streaming and cavitation process encourages uniform distribution [18] of SiC nanoparticles.

The fabricated samples were machined as per ASTM standard. The prepared test specimens were used for tensile, fracture and microstructure studies. Samples were polished on four different grades of emery papers, where disc polishing, etching, cleaning were the steps followed to prepare the sample for Optical Microscope (OM) and Scannin Electron Microscope (SEM) analysis. Initially the samples were hand polished on I/0, II/0, III/0 and IV/0 double coated emery papers. The direction of polishing changes from one grade to another. Alternatively, perpendicular directions were selected to eliminate all the hatching lines on the surface of the specimen. Then samples were disc polished for 10 min where aluminum oxidepowder was used for better surface finish. Mirror like finish was obtained after disc polishing. Now the samples were etched on the surface using Keller agent for 25–27 min, to elevate the grain boundaries on the surface by dissolving Al. The samples were then cleaned with acetone. Now the samples were ready for SEM and OM analysis. OM images were used to investigate the grain refinement of different nanocomposites and SEM for particle distribution as well as fracture surface analysis.

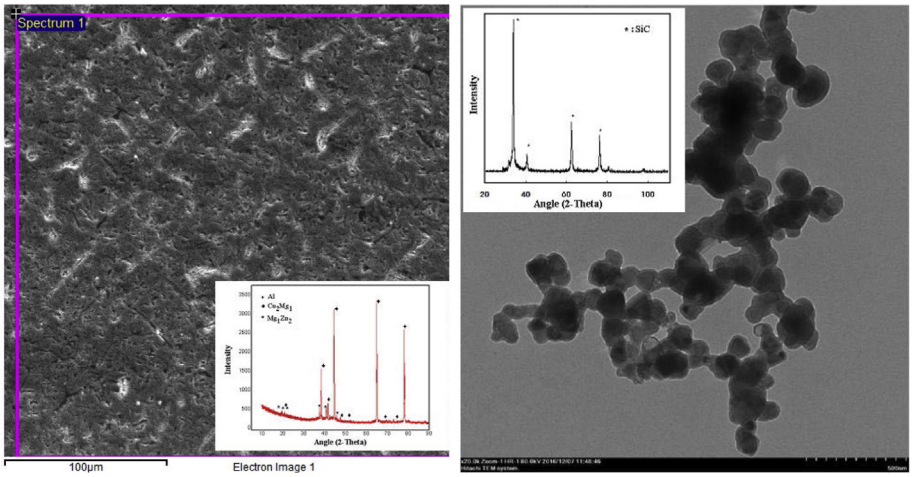

Fig. 3. (*a*) SEM and XRD analysis of AA7150, and (*b*)TEM and XRD image of SiC nanoparticles.

The density of various weight percentages of nano SiC reinforced composites were measured using Archimedes Principle. The weight of each sample was measured in air and distilled water using digital electronic balance (0.0001 g accuracy). The measured values were substituted in $\rho = \frac{w_1}{w_1 - w_2}$; where w1, and w2 represent the weight of the specimen in air and distilled water.

Porosity percentage of composite and base metal was estimated by the following formula "$porosity = [1 - \frac{\rho_{mc}}{\rho_m(1 - \frac{w\rho_{mc}}{\rho_p}) + w\rho_{mc}}] * 100$" Where ρ_p, ρ_m, ρ_{mc} are particle, matrix and nanocomposite densities, and 'w' is the weight fraction of reinforcement.

Vickers microhardness tester was used to measure the hardness of fabricated nanocomposites. A diamond indenter was used to indent the surface of samples and the Vicker hardness values were measured for ceramic reinforced samples of 0, 0.5, 1.0, 1.5, and 2.0 wt% of SiC nanocomposites. Testing was performed for 200 g applied load and dwell time of 15 s and experiments were repeated 5 times at different locations and the average values are reported in Table 1.

The tensile behaviour of various nanocomposites was tested on INSTRON universal testing machine at DRDO, Hyderabad as per ASTM E8M small standard. The sample size had 9 mm gauge diameter, 45 mm gauge length and 100 mm of total length. For each combination, the test was repeated 3 times and the average values figure in Table 1.

3. Results and discussion

3.1. Microstructure analysis

The impact of novel fabrication process and the effect of silicon carbide reinforcement on AA7150 alloy were examined. OM, SEM, and X-ray diffraction (XRD) were used to analyze AA7150 alloy and its composites AA7150-X wt.% SiC. Fig. 3a shows the microstructure and XRD analysis of aluminium 7150 alloy. Fig. 3b shows transmission electron microscopy photographs and XRD spectrum of SiC nanoparticles, which confirms good peak arrangement with reported values of "JCPDS X'Pert HighScore Plus" and AA7150 represents the high intensity peaks of Al, Cn_2Mg_1 and Mg_1Zn_2.

The grain refinement of a particle reinforced nanocomposite (Fig. 4) is a crucial strengthening mechanism because it improves the strength and fracture toughness of the composite at low-temperature conditions. The strengthening value is given by Hall Petch [19] formula ($\sigma_{hp} = \frac{K}{\sqrt{d}}$) where. 'K' is strength coefficient and 'd' is the grain size. Therefore the strength of the composite material is inversely proportional to the grain size of the material. Strengthening of grain refining takes place because of dislocation interactions with grain boundaries. SiC nanoparticles act as nucleation sites towards the matrix phase and limit the solidification procedure in composite material, which results in grain refinement. Therefore, the grain refinement of AA7150 increases the grain boundary density [20] and protects the movement of dislocations, which contribute to the strength in composite material. Grain refinement is enhanced with increase in the weight of ceramic reinforcement particles [21,22]. Fig. 4a–d shows the grain refinement of alloy matrix grains and reinforcement magnitude with the addition of second phase ceramic nanoparticles and it increases with an increase of weight percentage of SiC nanoparticles by up to 1.5 % in nanocomposites. Beyond 1.5 wt% of SiC, the grain size of the matrix increases (Fig. 4e) due to clusters/agglomerations, voids [23], and these are confirmed with SEM photograph (Fig. 5d).

The magnitude of grain refinement size was calculated through linear intercept method and ImageJ software [23]. The grain sizes were measured in the direction of principal planes and the calculated values were substituted in average grain size formula ($AGS = \frac{Length\ of\ Line}{No.\ of\ Grains}$), the values obtained are represented in Table 1 and the corresponding graphs are shown in Fig. 4f. From the result, it is observed that the percentage reduction in grain size is 57.9% compared to alloy matrix.

Fig. 5a–d shows electron micrographs of particle distribution with various weight percentages of SiC nanoparticle reinforced composites at as-cast material conditions. Energy dispersive X-ray spectroscopy (EDS) at 1.5 % SiC reveals information (Fig. 6) about elements and shows nanocomposites with major chemical elements such as Al, Mg, Zn, Cu and Si, carbon (C) as second phase elements. A high weight percentage of reinforcement mixing shows more probability of clusters/agglomerations, voids [24] and it is confirmed from Fig. 5d at 2% SiC reinforcement in AA7150. Fig. 5a–c demonstrate uniform distribution of nano SiC particles in the Al alloy matrix using the novel fabrication process. The distribution increases with increase in wt. %SiC. It is also noticed that porosity is decreasing with increasing weight percentage of SiC upto 1.5% due to ultrasonic degassing effect [17] and beyond 1.5%, it shows clusters and porosity due to high surface area to volume ratio.

XRD peaks of AA7150-SiC nanocomposites were examined on "Panalytical Xpert" X-ray powder diffractometer using Cu-K_α (λ = 1.54060 A°) radiation and the results are reported in Fig. 7. XRD was carried out with slow scan at a selected step size (0.005°), measuring time (5 s) and the angle (2Θ) maintained between 10°-80°. From the results of XRD spectrum, there are some smaller SiC nano-particulate peaks indicating beside angle (2Θ) 45°. It was also observed that the intensities of SiC peaks apparently increasing with increasing of wt. % SiC reinforcement content as well as reveals the elemental peaks such

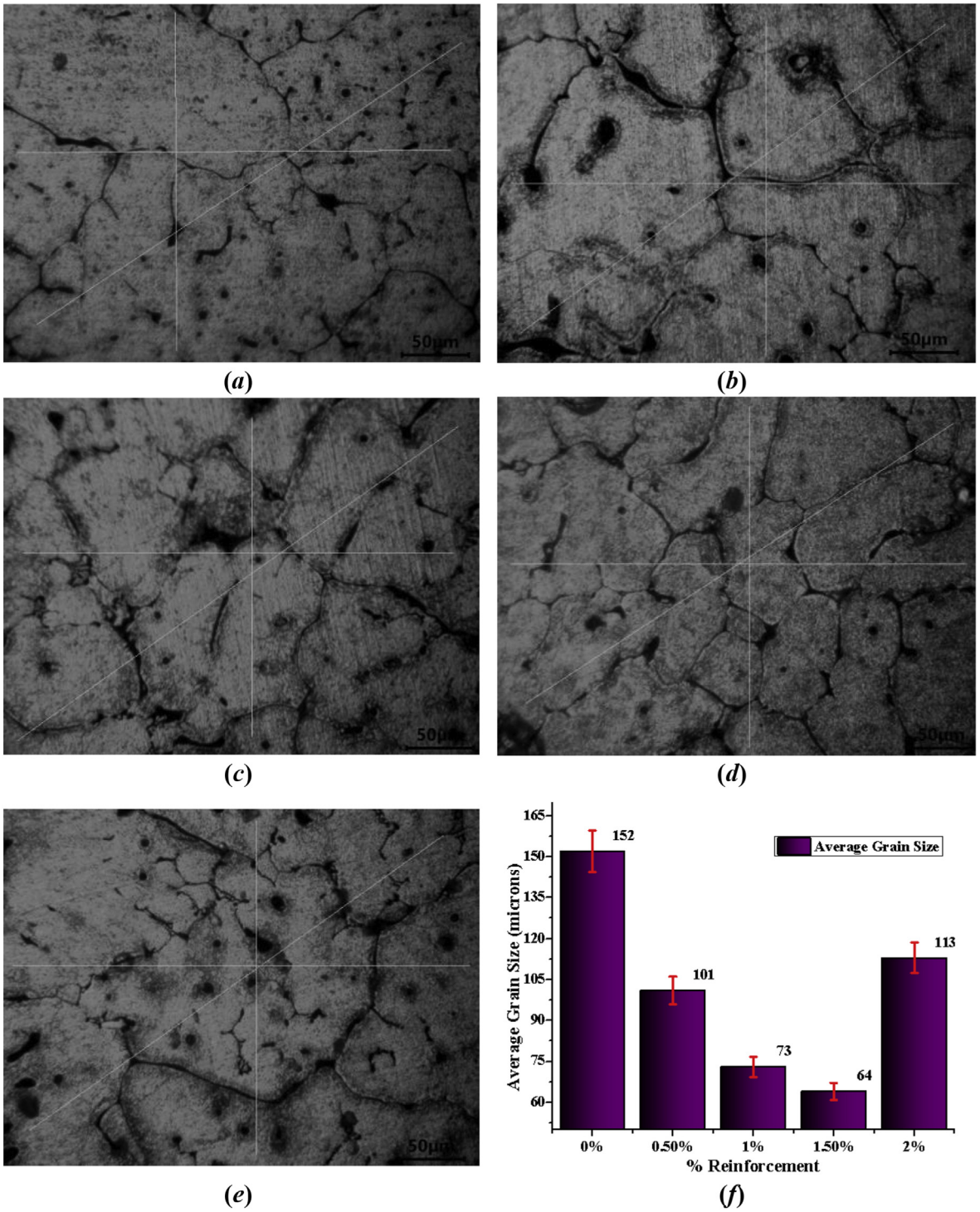

Fig. 4. Optical microscope images for grain refinement of (*a*) AA7150, (*b*) 0.5%SiC, (*c*) 1.0%SiC, (*d*) 1.5%SiC, (*e*) 2.0%SiC, and (*f*) Graphical representation of grain size.

as SiC (shorter peak) and Al (larger peak: AA7150) in the XRD spectrum.

3.2. Evaluation of material properties

The densities of nanocomposites were measured by careful experiments to determine the porosity level of the composite material; Archimedes principle was used to calculate density by considering the sample weight in air and its weight in distilled water; the nanocomposites were cut from nanocomposite blocks. Inadequate theoretical density of each nanocomposite material was calculated through rule of mixing method. The alloy matrix and SiC nanoparticles had densities of 2.83 g/cc and 3.216 g/cc respectively. It can be observed from the graph that the composite densities were enhanced compared to that of base alloy matrix. Further, experimental density increased (Fig. 8a) with increase in weight percentage of nano SiC [25] in the nanocomposites. These increments in experimental density of AA7150-SiC nanocomposites are primarily due to higher densities of SiC particles compared to AA7150 alloy material.

To find the porosity, the densities values based on experiments were

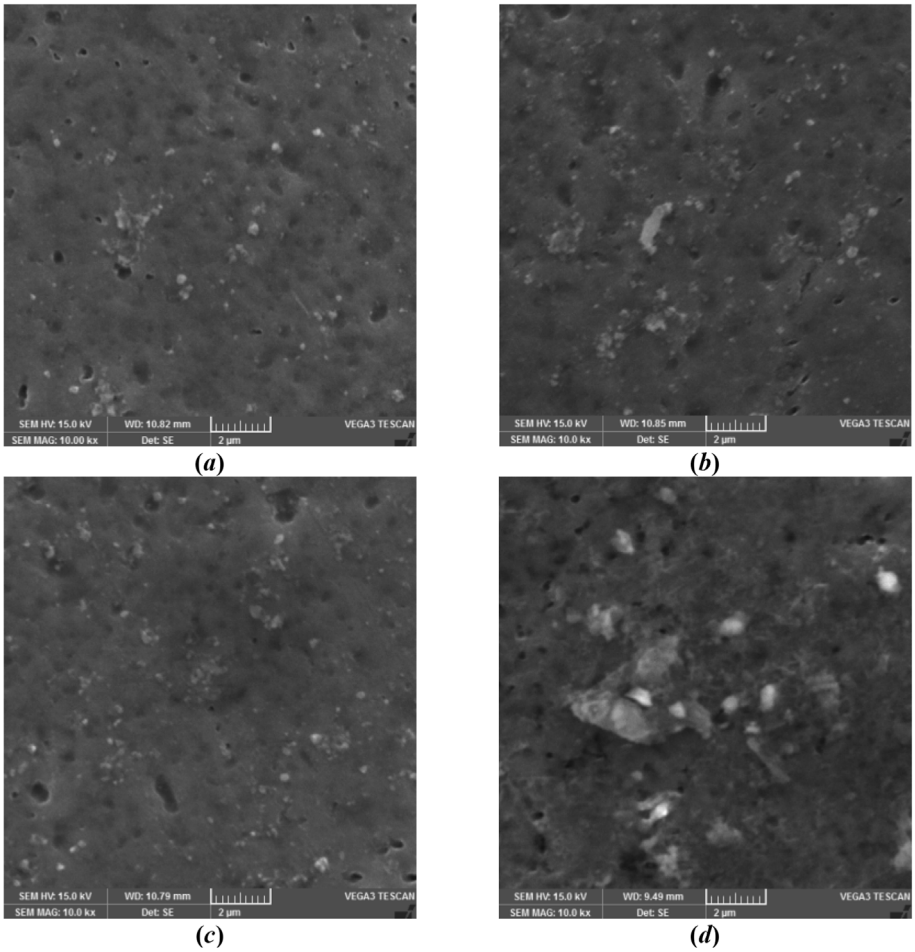

Fig. 5. SEM images for particle distribution of (*a*) 0.5%SiC, (*b*) 1.0%SiC, (*c*) 1.5%SiC, (*d*) 2.0%SiC.

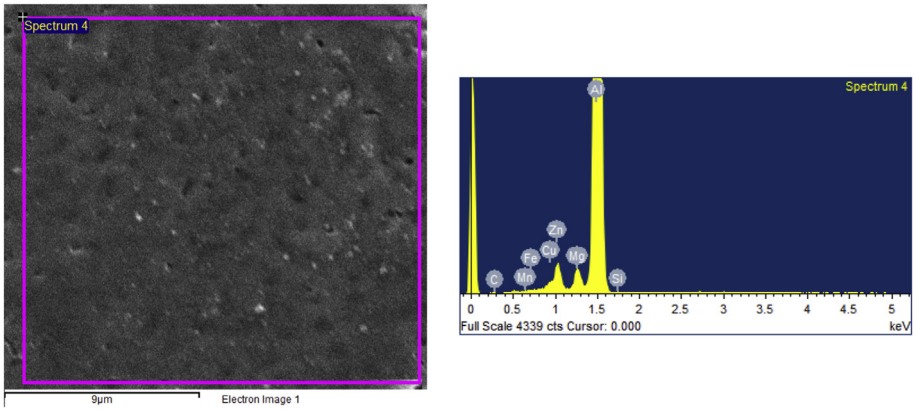

Fig. 6. EDS spectrum of AA7150–1.5 wt%SiC.

tested on base alloy matrix and matrix reinforced with SiC nanocomposites at as-cast state. The percentage of porosity after incorporation of SiC nanocomposites is represented in Fig. 8b. It is observed that the percentage of porosity decreases with an increase of SiC nanoparticles by up to 1.5% weight fraction due to ultrasonic degassing effect and uniform dispersion of nanoparticles. Further increase in reinforcement leads to increase in porosity due to large surface area to volume ratio of nanoparticles [26]. Once the limit is crossed in the molten pool, there is an improvement in the formation of clusters and voids resulting in more porosity. It is confirmed by Fig. 5d.

The microhardness of unreinforced and SiC reinforced nanocomposites were carried out through Vicker hardness tester at as-cast state. Each experiment was repeated 8 times and the mean of best 5 readings was calculated. The microhardness results are represented in a bar chart in Fig. 9. It is observed that the microhardness was enhanced and was greater than that of base alloy matrix. Microhardness was found to increase with an increase in weight percentage of nanoparticles [27] and it can be rightly attributed to ultrasonication, which leads to homogeneous mixing of SiC. The movement of dislocation is prevented by engulfed SiC nanoparticles as the indentor movement increases particle congregation near the indentor [28]. Hence, there is an increase in hardness of nanocomposites. And it is also due to tight

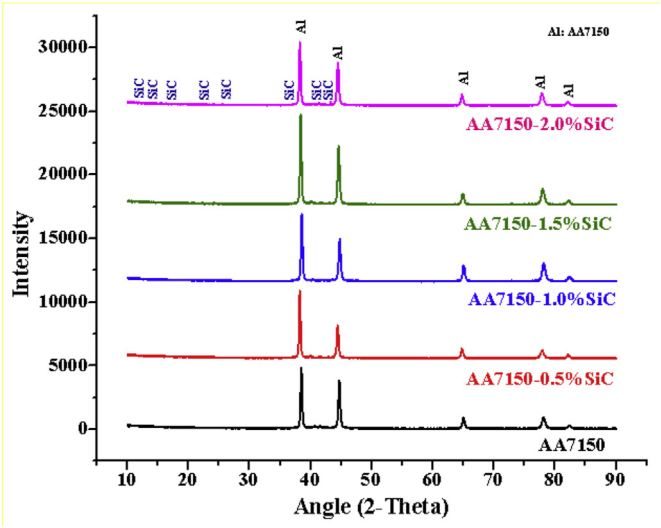

Fig. 7. XRD analysis of AA7150-SiC nanocomposites.

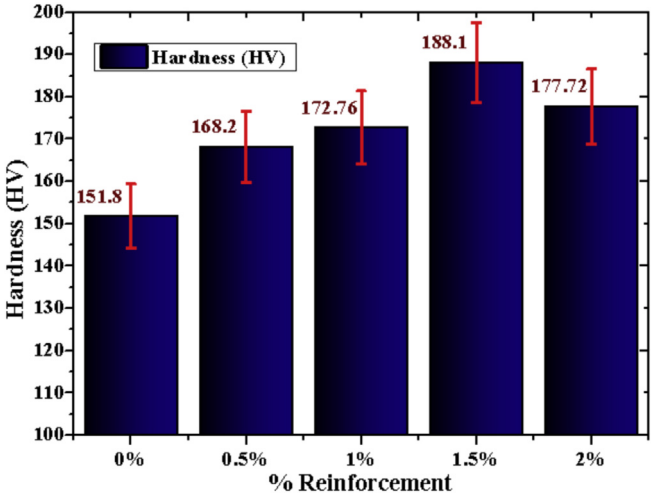

Fig. 9. Graphical representation of microhardness.

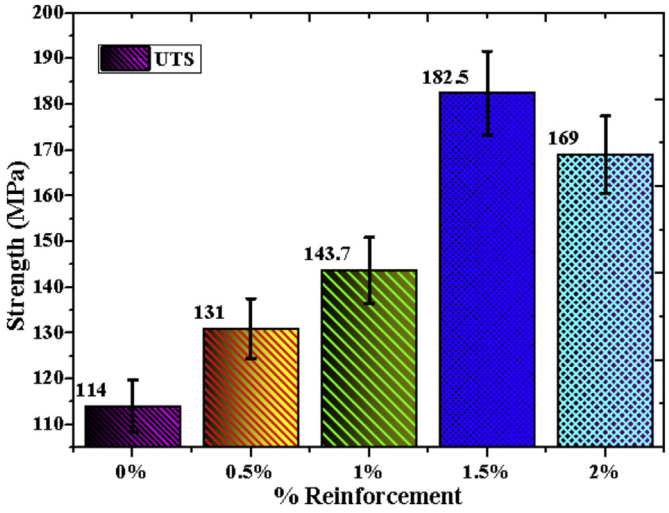

Fig. 10. Graphical representation of ultimate tensile strength.

adhesion between ceramic nanoparticles and alloy matrix as well as hard phase ceramic particles. Beyond 1.5%SiC, the microhardness of nanocomposite decreases due to higher grain size and clusters. It is confirmed in Figs. 4e & 5d.

Tensile test was carried out on Instron universal testing machine (UTM) for reinforced and unreinforced composites. The results are represented in Table 1. Fig. 10 shows the ultimate tensile strength variations against weight percentage of reinforcement and it is seen to increase with increase in SiC nanoparticles [29,30] up to 1.5% due to high dislocation between alloy matrix and nanoparticles, which leads to more dislocation loops around the reinforcement particles and produces back pressure that restricts the movement of dislocations as well as grain refinement, resulting in enhanced strength of nanocomposite. Beyond 1.5%, there is decrease in the strength of nanocomposite due to clusters/agglomerations, resulting in advancing the failure of nanocomposites and a consequent reduction in mechanical properties. This reduction is attributed to cluster/agglomeration present in the composite and creates high stress concentration [31,32] which leads to crack formation and further propagation, resulting in advancing the material properties.

SEM fractograph images of alloy matrix, at optimal strength (AA7150–1.5%SiC) and maximum reinforcement (AA7150-2%SiC) were taken from tensile fracture surface, as shown in Fig. 11. These images were captured at 200X magnification as well as the enlarged scale of 1000X magnification. Fig. 11a shows the fracture surface of AA7150 alloy matrix sample which shows large grape shape quantities as well as dendritic globules [33]. SiC reinforced nanocomposites (Fig. 11b and c) shows dendritic microstructure [34–36] and these act as a weak zone as well as stress riser which leading to crack initiation. These cracks spread around the dendritic boundaries which are due to the alloy matrix and ceramic particle interface, behaving like stress concentration spots. Micro-cracks are produced at interfaces as well which run through soft alloy matrix material and ceramic particles that show stepwise dendritic structure. The failure of SiC reinforced nanocomposites as the suitable alloy is confirmed with inter-dendritic,

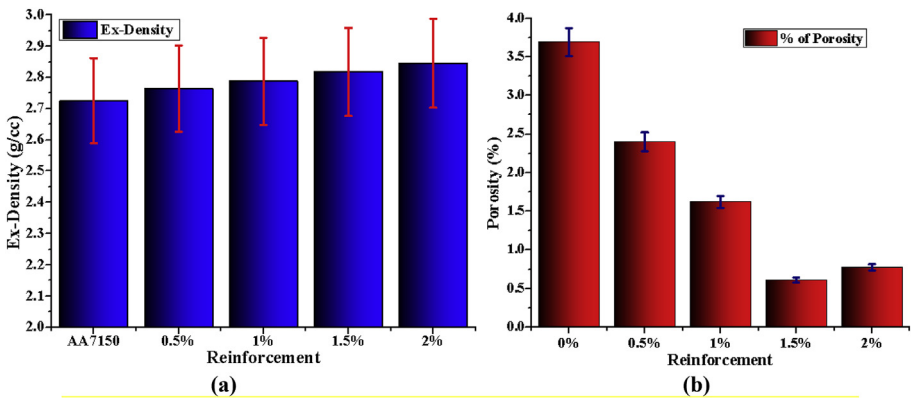

Fig. 8. Graphical representation of (a) Experimental density and (b) Porosity.

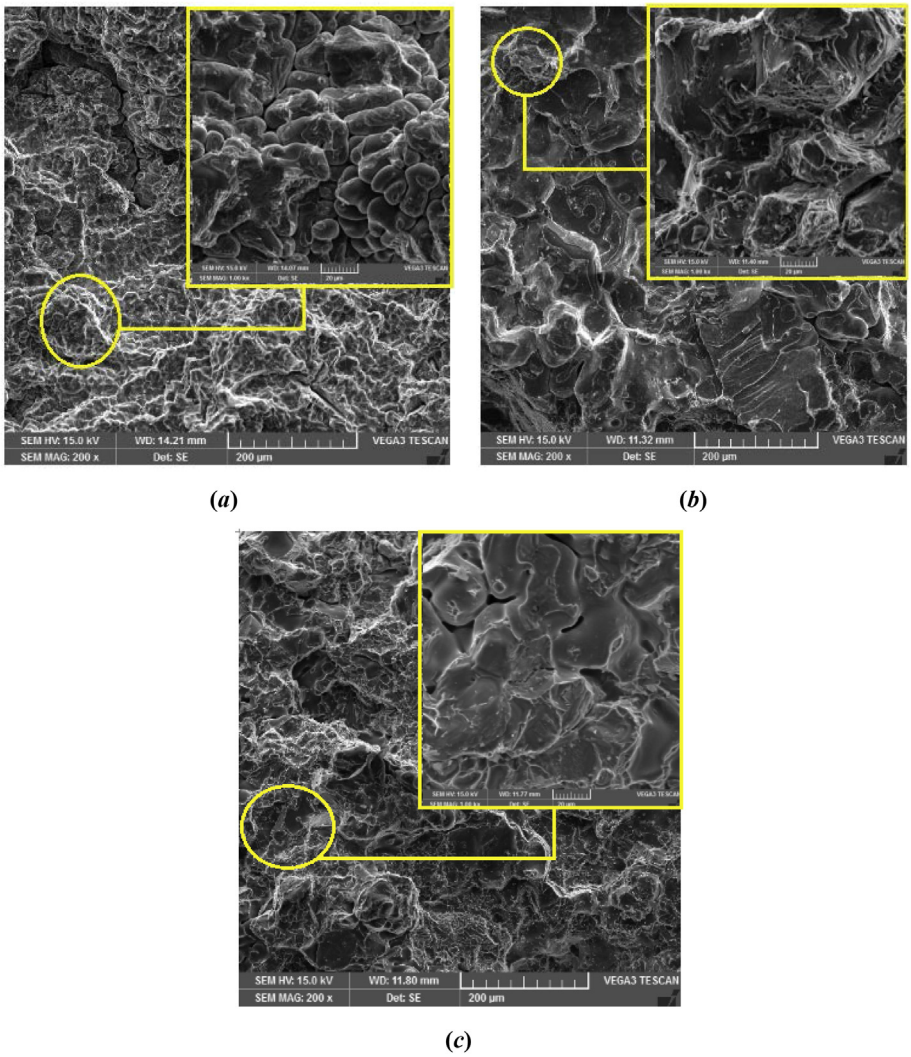

Fig. 11. SEM images for fracture surface of (*a*) AA7150, (*b*) AA7150-1.5 wt%SiC, and (*c*) AA7150-2 wt%SiC.

stepwise dendrites and transgranular cleavage facets on fracture surface fractographs as shown in Fig. 11b and c. It is also observed that the voids and micro-cracks are minimized at AA7150–1.5%SiC compared to base alloy and AA7150-2%SiC nanocomposite.

From the results and analysis, it is confirmed that the mechanical properties of AA7150-X wt.%SiC nanocomposite play a crucial role with respect to porosity, distribution and dispersion of nanoparticles throughout the material. Hence, the novel fabrication process was successfully developed based on a sequence of operations involving vortex, double stir casting, and ultrasonication methods to manufacture AA7150-X wt. %SiC nanocomposite and this process was achieved with minimum porosity and maximum homogeneous distribution of SiC nanoparticles.

4. Conclusions

A novel fabrication process was successfully introduced to enhance nanoparticle distribution and improve the performance of AA7150-SiC nanocomposites. The microstructure and mechanical properties were evaluated. The optical microstructure analysis revealed grain refinement and it increased with an increase in SiC nanoparticles and maximum refinement was observed at 1.5 wt%SiC. SEM photographs confirm uniform distribution of SiC nanoparticles. The mechanical properties of AA7150–1.5 wt%SiC exhibit significant improvement as compared to counter parts and it reveals an enhancement of 23.9% (151.8–188.1 H V) in microhardness, 60.1% (117–182.5 MPa) in ultimate tensile strength and minimum porosity (83.47% reduction) at 1.5 wt%SiC as compared to matrix alloy.

Acknowledgments

“I would like to thank Dr. M Raja Vishwanathan, Head of Humanities & Social Science Department, National Institute of Technology, Warangal, Telangana, India, for proofreading the paper and for his useful suggestions”.

References

[1] D.K. Koli, G. Agnihotri, R. Purohit, A review on properties, behaviour and processing methods for Al- nano Al2O3 composites, Procedia Mater. Sci. 6 (2014) 567–589, https://doi.org/10.1016/j.mspro.2014.07.072.
[2] A. Bahrami, N. Soltani, M.I. Pech-Canul, Effect of sintering temperature on tribological behavior of Ce-TZP/Al2O3-aluminum nanocomposite, J. Compos. Mater. 49 (2015) 3507–3514, https://doi.org/10.1177/0021998314567010.
[3] N. Soltani, M.I. Pech-Canul, A. Bahrami, Effect of 10Ce-TZP/Al2O3 nanocomposite particle amount and sintering temperature on the microstructure and mechanical properties of Al/(10Ce-TZP/Al2O3) nanocomposites, Mater. Des. 50 (2013) 85–91, https://doi.org/10.1016/j.matdes.2013.03.001.
[4] S.A. Sajjadi, M.T. Parizi, H.R. Ezatpour, A. Sedghi, Fabrication of A356 composite reinforced with micro and nano Al2O3 particles by a developed compocasting method and study of its properties, J. Alloys Compd. 511 (2012) 226–231, https://doi.org/10.1016/j.jallcom.2011.08.105.
[5] A. Mazahery, M.O. Shabani, Mechanical properties of A356 matrix composites

reinforced with nano-SiC particles, Strength Mater. 44 (2012) 686–692, https://doi.org/10.1007/s11223-012-9423-0.
[6] Mehrdad Shayan, Beitallah Eghbali, Behzad Niroumand, Synthesis of AA2024-(SiO2np + TiO2np) hybrid nanocomposite via stir casting process, Mater. Sci. Eng. A 756 (2019) 484–491, https://doi.org/10.1016/j.msea.2019.04.089.
[7] H.U. Kun, Yuan Du, L.Ü. Shu-lin, W.U. Shu-sen, Effects of nano-SiCp content on microstructure and mechanical properties of SiCp/A356 composites assisted with ultrasonic treatment, Trans. Nonferrous Metals Soc. 28 (2018) 2173–2180, https://doi.org/10.1016/S1003-6326(18)64862-9.
[8] Xuan Liu, Cheng Zhang, Zhi-qiang Zhang, Ji-lai Xue, Le Qi-chi, The role of ultrasound in hydrogen removal and microstructure refinement by ultrasonic argon degassing process, Ultrason. Sonochem. 38 (2017) 455–462, https://doi.org/10.1016/j.ultsonch.2017.03.041.
[9] Xiong Yang, W.U. Shu-sen, L.Ü. Shu-lin, Hao Liang-yan, Fang Xiang-gang, Refinement of LPSO structure in Mg-Ni-Y alloys by ultrasonic treatment [J], Ultrason. Sonochem. 40 (2018) 472–479, https://doi.org/10.1016/j.ultsonch.2017.07.042.
[10] Lin Chong, W.U. Shu-sen, Zhong Gu, Li Wan, Ping An, Effect of ultrasonic vibration on Fe-containing intermetallic compounds of hypereutectic Al−Si alloys with high Fe content, Trans. Nonferrous Metals Soc. 23 (2013) 1245–1252, https://doi.org/10.1016/S1003-6326(13)62589-3.
[11] Abdolreza Javadi, Jingzhou Zhao, Chezheng Cao, Marta Pozuelo, Yingchao Yang, Injoo Hwang, Ting Chang Lin, Xiaochun Li, Stretching micro metal particles into uniformly dispersed and sized nanoparticles in polymer, Nature-Sci. Rep. 7 (2017) 7098, https://doi.org/10.1038/s41598-017-07788-3.
[12] Amin Bahrami, Niloofar Soltani, I. Martin, Pech-Canul, Shaghayegh Soltani, Luis A. González, Carlos A. Gutiérrez, Joshua Tapp, Angela Möller, Aleksander Gurlo, Bilayer graded Al/B4C/rice husk ash composite: wettability behavior, thermo-mechanical, and electrical properties, J. Compos. Mater. 52 (2018) 3745–3758, https://doi.org/10.1177/0021998318769993.
[13] Yuan Du, Xiong Yang, Shusen Wu, Lü Shulin, Kun Hu, Development of high strength and toughness nano-SiCp/A356 composites with ultrasonic vibration and squeeze casting, J. Mater. Process. Technol. 292 (2019) 1–9, https://doi.org/10.1016/j.jmatprotec.2019.01.021.
[14] A.J. Knowles, X. Jiang, M. Galano, et al., Microstructure and mechanical properties of 6061 Al alloy based composites with SiC nanoparticles, J. Alloys Compd. 615 (2014) S401–S405, https://doi.org/10.1016/j.jallcom.2014.01.134.
[15] L. Kollo, C.R. Bradbury, R. Veinthal, et al., Nano-silicon carbide reinforced aluminium produced by high-energy milling and hot consolidation, Mater. Sci. Eng. A 528 (2011) 6606–6615, https://doi.org/10.1016/j.msea.2011.05.037.
[16] J.Y. Li, F. Li, S.S. Wu, Lü Shulin, Wei Guo, Xiong Yang, Variation of microstructure and mechanical properties of hybrid particulates reinforced Al-alloy matrix composites with ultrasonic treatment, J. Alloys Compd. 789 (2019) 630–638, https://doi.org/10.1016/j.jallcom.2019.03.074.
[17] Amir Hussain Idrisi, Abdel-Hamid Ismail Mourad, Conventional stir casting versus ultrasonic assisted stir casting process: mechanical and physical characteristics of AMCs, J. Alloys Compd. 805 (2019) 502–508, https://doi.org/10.1016/j.jallcom.2019.07.076.
[18] Pagidi Madhukar, N. Selvaraj, Raghavendra Gujjala, Chilakalapalli Surya Prakasa Rao, Production of high performance AA7150-1% SiC nanocomposite by novel fabrication process of ultrasonication assisted stir casting, Ultrason. Sonochem. 58 (2019) 104665, https://doi.org/10.1016/j.ultsonch.2019.104665.
[19] A. Sanaty-Zadeh, P.K. Rohatgi, Corrigendum to: comparison between current models for the strength of particulate-reinforced metal matrix nanocomposites with emphasis on consideration of Hall–Petch effect, Mater. Sci. Eng. A 531 (2012) 112–118, https://doi.org/10.1016/j.msea.2011.10.043.
[20] C. Kannan, R. Ramanujam, Effectiveness evaluation of molten salt processing and ultrasonic cavitation techniques during the production of aluminium based hybrid nanocomposites - an experimental investigation, J. Alloys Compd. 751 (2018) 183–193, https://doi.org/10.1016/j.jallcom.2018.04.112.
[21] G. Gautam, N. Kumar, A. Mohan, Strengthening mechanisms of (Al3Zrmp + ZrB2np)/AA5052 hybrid composites, J. Compos. Mater. 50 (2016) 4123–4133, https://doi.org/10.1177/0021998316631811.
[22] Xuan Yang, Laurentiu Nastac, The role of ultrasonic cavitation in refining the microstructure of aluminum based nanocomposites during the solidification process, Ultrasonics 83 (2018) 94–102, https://doi.org/10.1016/j.ultras.2017.06.023.
[23] Dapeng Jiang, Jiakang Yu, Fabrication of Al2O3/SiC/Al hybrid nanocomposites through solidification process for improved mechanical properties, Metals 8 (2018) 572, https://doi.org/10.3390/met8080572.
[24] Mehrdad Shayan, Beitallah Eghbali, Behzad Niroumand, Synthesis of AA2024-(SiO2np + TiO2np) hybrid nanocomposite via stir casting process, Mater. Sci. Eng. A 756 (2019) 484–491, https://doi.org/10.1016/j.msea.2019.04.089.
[25] E. Bahmani, A. Abouei, V. Shajari, Y.S.H. Razavib, O. Bayat, Investigation on microstructure, wear behavior and microhardness of Al−Si/SiC nanocomposite, Surf. Eng. Appl. Electrochem. 54 (2018) 350–358, https://doi.org/10.3103/S1068375518040038.
[26] P. Madhukar, N. Selvaraj, C.S.P. Rao, Manufacturing of aluminium nano hybrid composites: a state of review, Mater. Sci. Eng. 149 (2016) 12114 https://iopscience.iop.org/article/10.1088/1757-899X/149/1/012114/pdf.
[27] Pagidi Madhukar, N. Selvaraj, C.S.P. Rao, G.B. Veeresh Kumar, Tribological behavior of ultrasonic assisted double stir casted novel nano-composite material (AA7150-hBN) using Taguchi technique, Composites Part B 175 (2019) 107136, https://doi.org/10.1016/j.compositesb.2019.107136.
[28] Shu-sen Wu, Yuan Du, Lü Shu-lin, Kun Hu, Ping An, Nano-SiCP particles distribution and mechanical properties of Al-matrix composites prepared by stir casting and ultrasonic treatment, china foundry 15 (2018) 203–209, https://doi.org/10.1007/s41230-018-8009-2.
[29] A. Melaibari, A. Fathy, M. Mansouri, M.A. Eltaher, Experimental and numerical investigation on strengthening mechanisms of nanostructured Al-SiC composites, J. Alloys Compd. 774 (2019) 1123–1132, https://doi.org/10.1016/j.jallcom.2018.10.007.
[30] Xiao fan Du, Tong Gao, Zhao Qian, Yuying Wu, Xiangfa Liu, The in-situ synthesis and strengthening mechanism of the multi-scale SiC particles in Al-SiC alloys, J. Alloys Compd. 750 (2018) 935–944, https://doi.org/10.1016/j.jallcom.2018.04.006.
[31] Z. Wang, K. Georgarakis, K.S. Nakayama, Y. Li, A.A. Tsarkov, G. Xie, D. Dudina, D.V. Louzguine-Luzgin, A.R. Yavari, Microstructure and mechanical behavior of metallic glass fiber reinforced Al alloy matrix composite, Nature-Sci. Rep. 6 (2016) 24384, https://doi.org/10.1038/srep24384.
[32] A. Bahrami, N. Soltani, S. Soltani, M.I. Pech-Canul, L.A. Gonzalez, C.A. Gutierrez, A. Möller, J. Tapp, A. Gurlo, Mechanical, thermal and electrical properties of monolayer and bilayer graded Al/SiC/rice husk ash (RHA) composite, J. Alloys Compd. 699 (2017) 308–322, https://doi.org/10.1016/j.jallcom.2016.12.339.
[33] O.B. Bembalge, S.K. Panigrahi, Development and strengthening mechanisms of bulk ultrafine grained AA6063/SiC composite sheets with varying reinforcement size ranging from nano to micro domain, J. Alloys Compd. 766 (2018) 355–372, https://doi.org/10.1016/j.jallcom.2018.06.306.
[34] A.V. Pozdniakov, V.S. Zolotorevskiy, R.Yu. Barkov, A. Lotfy, A.I. Bazlov, Microstructure and material characterization of 6063/B4C and 1545K/B4C composites produced by two stir casting techniques for nuclear applications, J. Alloys Compd. 664 (2016) 317–320, https://doi.org/10.1016/j.jallcom.2015.12.228.
[35] X.X. Zhang, H.M. Wei, A.B. Li, Y.D. Fu, L. Geng, Effect of hot extrusion and heat treatment on CNTs–Al interfacial bond strength in hybrid aluminium composites, Compos. Interfac. 20 (2013) 231–239, https://doi.org/10.1080/15685543.2013.793093.
[36] J. Li, S. Lü, S. Wu, Q. Gao, Effects of ultrasonic vibration on microstructure and mechanical properties of nano-sized SiC particles reinforced Al-5Cu composites, Ultrason. Sonochem. 42 (2018) 814–822, https://doi.org/10.1016/j.ultsonch.2017.12.038.